LA-UR 89-1751

CONF-8907205--1

Los Alamos National Laboratory is operated by the University of California for the United States Department of Energy under contract W-7405-ENG-36

LA-UR--89-1751

DE89 012582

TITLE PHYSICS WITH ETA MESONS

AUTHOR(S) Lon-chang Liu

SUBMITTED TO Proceedings of The Third International Symposium on Pion-Nucleon and Nucleon-Nucleon Physics

DISCLAIMER

Los Alamos Los Alamos National Laboratory
Los Alamos, New Mexico 87545

FORM NO. 836 R4
ST. NO. 2629 5/81

PHYSICS WITH ETA MESONS

Lon-chang Liu
Los Alamos National Laboratory
Los Alamos, NM 87545, U.S.A.

I. INTRODUCTION

Since the advent of pion factories, an impressive amount of information about the nuclear dynamics of the $\Delta(1232)$ pion-nucleon resonance has been obtained. The study of this isospin-3/2 resonance has greatly benefited from the fact that π^-n and π^+p systems are pure I=3/2 states, which couple only to the Δ in the resonance region. Such isospin selectivity of the pion does not exist, however, for the I=1/2 N* resonances because it is not possible to form a pure I=1/2 state with a pion and a nucleon. Eta mesons have zero isospin. Consequently, the ηN systems are in a pure I=1/2 state, and η can be used to tag those N* resonances to which it strongly couples. In Sec. II, we will briefly review the ηN interaction from the threshold region to c.m. energy $\sqrt{s} \approx 1600$ MeV. We shall see how improved πN data can help the study of ηN interactions. In Sec.III, I shall discuss what new information about the hadronic interaction can be learned from the study of eta production in pp collisions. The behavior of eta meson in nuclei will be the subject of Sec.IV. The interesting question of the quark structure of $\eta(549)$ and $\eta'(958)$ will be discussed in Sec.V within the framework of a simple model.

II. ETA-NUCLEON INTERACTION

Pion-induced η production on a free nucleon is an important πN reaction in the energy region T_π=0.6-1.0 GeV. It is the second most important πN inelastic channel, second only to π-induced π production. The threshold for the reaction $\pi^-p \to \eta n$ on a free proton is at T_π=551 MeV or $\sqrt{s}$=1488 MeV. The total production cross section rises rapidly with pion energy and reaches a maximum of 2.5 mb at T_π=661 MeV or $\sqrt{s}$=1550 MeV.(Fig.1.) In this threshold region, the bulk of the η production in the πN collision is likely to be due to the formation of N*(1535) as a doorway state, which then decays into an η and a nucleon. In Table I, we list the

decay branching ratios of some well-established N* resonances. An inspection of this table indicates that:

(a) Below 1600 MeV, there are only three important reaction channels, the πN, ηN, and the $\pi\pi N$ channels;

(b) In this low-energy region, the ηN system couples most strongly to the N*(1535) resonance;

(c) In the region 1600-1700 MeV, two additional reaction channels, the ΛK and ΣK, become important;

(d) The $\eta(549)$-N system couples appreciably only to a few of the N* resonances, and there is no clear evidence of strong coupling between N* and $\eta'(958)$.

Table I. Branching Ratios of N* Resonances

Resonances			πN	ηN	$\pi\pi N$	ΛK	ΣK
N*(1440)	$1/2^+$	P11	50-70		30-50		
N*(1520)	$3/2^-$	D13	50-60	~0.1	40-50		
N*(1535)	$1/2^-$	S11	35-50	45-55	10		
N*(1650)	$1/2^-$	S11	55-65	~1.5	20-35	~8	
N*(1675)	$5/2^-$	D15	35-40	~1	60-65	~0.1	
N*(1680)	$5/2^+$	F15	55-65	<1	35-45		
N*(1700)	$3/2^-$	D13	5-15	~4	80-90	~0.2	
N*(1710)	$1/2^+$	P11	10-20	25	<50	15	2-10
N*(1720)	$3/2^+$	P13	10-20	~3.5	<75	~5	2-5
N*(2190)	$7/2^-$	G17	14	~3		~0.3	
N*(2220)	$9/2^+$	H19	18	~0.5		~0.2	
N*(2250)	$9/2^-$	G19	10	~2		~0.3	

The large difference between the ηN decay branching ratios of the N*(1535) and N*(1650) is noteworthy, especially because these two N* have the same quantum number. Is this difference due to simple kinematical reasons, namely, that the N*(1650) is situated just above the ΛK threshold so that the phase-space factor suppresses the ηN branch in favor of ΛK or because is it due to a difference between the basic quark structures of these two N*? While it is important to understand the N*'s and their decays at the quark-gluon level[1], one should also note that the description of the $N^* \to \eta N$ decay belongs to the regime of non-perturbative QCD, for which theoretical results are very model-dependent. For this reason, it is also useful to address these same issues at the hadronic level and confront the results obtained in the latter approach to those given by the quark models.

We have proposed a coupled-channel isobar model for πN, ηN, and $\pi\pi N$ systems in the energy domain below 1600 MeV [2]. In this model, the reactions proceed through the formation of an N* doorway state; the N*(1440)P11, N*(1520)D13, and N*(1535)S11 were used as the dynamical sources of the p-, d- and s-wave interactions, respectively. The various coupling constants and range parameters of the model were determined from the published πN P11, D13, and S11 phase shifts alone.

Although the ηN branching ratios and the $\pi^- p \to \eta n$ cross sections were not used in the parameter search, they were satisfactorily reproduced by the model. In Figs. 1 and 2, we present, respectively, the theoretical total and differential cross sections with the data[3,4]. The $\pi N \to \eta N$ c.m. differential cross section has the form

$$d\sigma/d\Omega = |f(\theta)|^2 + |g(\theta)|^2, \tag{1}$$

where the spin-nonflip and spin-flip amplitudes are given by

$$f(\theta) = K[T_S + T_P \cos\theta + 2T_D P_2(\cos\theta)] \tag{2}$$

$$g(\theta) = K\sin\theta[T_P + 3T_D \cos\theta], \tag{3}$$

and K is a kinematical factor[2]. Clearly the differential cross section due to T_S alone will be angle-independent. If only T_S and T_P are used, then the cross sections can only have a linear dependence on $\cos\theta$. On the other hand, the cross section given by T_D alone has a minimum at $\theta = 90^\circ$, making it obvious that s-, p-, and d-wave N* resonances are all needed in describing the data. Calculated total cross sections are given in Fig.1. It is clear that the model is not good for the higher-energy regime where the hyperon channels and more N* have to be included in the analysis. Such analysis is tedious but feasible. The quality of the fit to πN phase shifts are shown in Figs. 3-5 for two typical sets of phase shifts (the VPI[5] and CERN theoretical[6]). The two chosen sets of phase shifts have the largest difference in the S11 channel. However, as indicated by Fig.2, calculated differential cross sections for the $\pi^- p \to \eta n$ reaction are

relatively insensitive to the use of model parameters determined from different πN phase-shifts.

On the other hand, calculated polarizations in the final state for an initially unpolarized system or the left-right symmetry $(N_L-N_R)/(N_L+N_R)$ produced by the polarized-spin target

$$P=\frac{2\mathrm{Im}(f^*g)}{|f|^2+|g|^2} \tag{4}$$

exhibits notable dependence on the πN phase shifts[7] (Fig.6). Polarization measurements of the $\pi^-p\to\eta n$ reaction can, therefore, provide additional constraints on πN phase-shift analyses.

The Lagrangians for the ηN→N*(1535) and πN→N*(1535) interactions can be written as $L=-f_{\eta NN^*}\,\bar{\psi}_{N^*}\psi_N\phi_\eta v(p^2)$ and $L=-f_{\pi NN^*}\,\bar{\psi}_{N^*}\psi_N\vec{\phi}_\pi\cdot\vec{\tau}v(p^2)$, where the form factors v=1 for an on-shell meson. From Ref.2 we have $f_{\eta NN^*}=2.07$ (resp. 1.46) and $f_{\pi NN^*}=0.87$ (resp. 0.70) for the VPI (resp. CERN-Th) input. (The f's are related to the g's of Ref.2 by $f^2=\alpha g^2(2\pi^2\omega_M/\sqrt{s})\Lambda^4/(\Lambda^2+\vec{p}_M^{\,2})^2$, where ω_M and $\vec{p}_M$ are the meson energy and momentum resulted from the decay of N*(1535), and α=1 for M=η and α=1/3 for M=π.)

In Fig.7, we show the ηN total and elastic cross sections. The divergence of the σ_{tot} at the threshold reflects the fact that the ηN→πN reaction is always energetically possible. Clearly, this threshold behavior invalidates the use of additive quark models to estimate the ηN total cross section. We note the lack of resonance structure in the energy dependence of the elastic cross sections. In fact, we have also noted that the apparent peaking of the $\pi^-p\to\eta n$ production cross section in this energy region (Fig.1) is due to the threshold phase-space ($k_{\eta n}/k_{\pi p}$) effect.

III. ETA PRODUCTION IN PP COLLISIONS

The threshold for the pp→ppη reaction is at T_p=2.42 GeV or $\sqrt{s}$= 1.255 GeV. The simplest reaction mechanism is the exchange of a π^0 and/or a ρ^0 (Fig.8). While the $\pi^0p\to\eta p$ amplitude is known from the $\pi^-p\to\eta n$ amplitude by isospin symmetry, the $\rho^0p\to\eta p$ amplitude is not known. Thus, η production by pp collisions can be used to determine the ρN→N* vertex.

In Fig.8, we compare the calculated cross sections with the existing data[8]. The dot-dashed curve is given by the π exchange alone while the dashed curve includes also the ρ exchange. In our calculation[9], we have assumed the relation $g_{\rho NN^*}/g_{\pi NN^*}=g_{\rho NN}/g_{\pi NN}$ and have used a $\Lambda_{\rho NN^*}$= 1 GeV/c. While it is possible to change the ρNN* coupling constant to fit the data, it is important to examine the contributions of higher-order mechanisms involving multiple Δ and/or N* excitations in the intermediate states and the convergence of this multiple excitation series. The full results will be reported in the near future.

In Fig.9, we show the relative contributions due to N*(1535)S11, N*(1440)P11, and N*(1520)D13 in the one π exchange mechanism. Clearly, the contribution by N*(1535) is the dominant one.

IV. ETAS IN NUCLEI

One interesting feature of η in nuclei is that it could be captured in principle, by the strong-interaction force into a nuclear orbital and form an eta-nucleus bound system or an η-mesic nucleus[10]. Because the threshold for ηN scattering (1488 MeV) is situated just below the N*(1535) resonance, the low-energy ηN interaction is attractive. This attraction was indeed borne out by coupled-channel analyses[2]. Although the attraction is insufficient to bind an η onto a free nucleon, it becomes sufficient to bind an η into a nucleus having a mass number greater than 11. Because the bound-state cross section in single-arm measurements of the (π^+,p) reaction is very small[11,12], Lieb et al. have searched for this possibility by using the $(\pi^+,pp\pi)$ reactions on Li, C, O, and Al targets [13]. They detected the fast, forward-going protons in coincidence with the expected η-mesic nucleus decay products in order to reduce the background. Assuming the bound state would decay via the process ηN→N*→πN, they detected the ppπ in coincidence between the forward ($\theta<30^o$) protons, the pions at 90^o, and the secondary protons emitted within a "back-to-back" cone with respect to the pion. Preliminary results show evidence that the η bound state may have been produced[13]. Fig.10 shows a summed spectrum of forward protons obtained from the oxygen target. The threshold of free η production is at T_p=105 MeV. Hence, the peak to the right of this threshold indicates the formation of η-mesic ^{15}O. Lieb et al. did not

find such peak in Li and C targets. Analysis of data from the aluminium target is still in progress. We are watching on the developments in their analysis with great interest.

To illustrate the size of η-mesic nuclei, we present in Fig.11 the 1s bound-state wave function of the eta in ^{15}O. This wave function give rises a r.m.s radius≈3.2 fm for the 1s orbital. The very long tail of the wave function further reflects the loose binding of the η in ^{15}O.

If the existence of the bound state is confirmed, then the binding energy and width of these states will provide another sensitive measurement of η and N* dynamics. We have investigated the modification of the ηN interaction in the nuclear matter. In our isobar model, this amounts to making self-energy insertions to the pion, eta, and nucleon, which form the N*, shown as the blobs in Fig.12. For the pion (resp. eta), we have summed the ring diagrams giving particle-hole and delta (resp. N*)-hole contributions. Further, we have normalized these contributions with the inclusion of short-range repulsion in particle-hole interaction, using a Migdal parameter equal to 0.7. (See Fig.13.) Results are presented in Table II where we give the calculated η binding energy in ^{15}O as a function of the nuclear density and of the nuclear N* potential strength.

Table II. Calculated Binding Energies of η in ^{15}O

	V(N*)=0	V(N*)=-60 (MeV)
Free Space	-(2.65+4.77i)	
0.7 ρ_o	-(1.36+6.47i)	-(12.5+15.2)
0.8 ρ_o	-(1.14+7.20i)	-(7.76+16.5)

We see that nuclear medium weakens the binding and increases the width. On the other hand, an additional attraction due to N*-nucleus interaction can enhance the binding although it also increases the width.

V. STRUCTURE OF η and η′

There is difficulty in explaining the η-η′ mass difference within the frame work of SU(3) symmetry. The non-existence of a low-mass isosinglet pseudoscalar meson has been suggested as an indication of a possible coupling of this meson to heavy quarks via the two-gluon intermediate state[14,15]. Models have been proposed in the literature to resolve this difficulty, invoking either the mixing of a $c\bar{c}$ component[16] or a gluonic

component[17] into both the η and η' mesons. In this sense, we regard the ηNN^* coupling constant determined from $\pi N \to \eta N$ reactions as an effective one. In the $c\bar{c}$ model, the wave functions of the η and η' can be written as

$$\eta = a_u(u\bar{u}+d\bar{d}) + a_s\, s\bar{s} + a_c\, c\bar{c}, \tag{5}$$

$$\eta' = b_u(u\bar{u}+d\bar{d}) + b_s\, s\bar{s} + b_c\, c\bar{c}. \tag{6}$$

There are similar expressions in the gluon model, in which the coefficients a_c and b_c are, respectively, replaced by a_g and b_g. A good place to differentiate these models is, for example, in the high-energy and high-momentum transfer $e^+e^- \to h+....$ reactions, where $h=\eta$ or η'. The multiplicity-ratio $R=\langle\eta\rangle/\langle\eta'\rangle$ for e^+e^- annihilation is given in the parton model by

$$R=\frac{\langle(4/9)(D_u^{\eta}(z)+D_c^{\eta}(z))+(1/9)(D_s^{\eta}(z)+D_d^{\eta}(z))\rangle}{\langle(4/9)(D^{\eta'}_u(z)+D^{\eta'}_c(z))+(1/9)(D^{\eta'}_s(z)+D^{\eta'}_d(z))\rangle}, \tag{7}$$

where the D's are Feynman quark decay (or fragmentation) functions. Following Field and Feynman[18] and assuming exact SU(4) symmetry, we can rewrite Eq.(7) to a good approximation as

$$R=\frac{5a_u^2+a_s^2+4a_c^2}{5b_u^2+b_s^2+4b_c^2}. \tag{8}$$

Using the wave functions of η and η' of Ref.16, we obtain R=0.72. Standard SU(3) wave functions give R=1.52. Experiment[19] gives R=2.5±1.3. In the gluon model, R can be written in a form similar to Eq.(8) with $4a_u^2$ and $4b_u^2$ being dropped. The model of Ref.17 then gives R=3.33. The above simple analysis seems to rule out the $c\bar{c}$ model. Although the standard SU(3) model gives an R in agreement with the data, it can not explain the η-η' mass

difference. Detailed results involving gluon content for the eta mesons will be reported elsewhere.

We point out that explicit gluonic wave functions have so far not been included in the quark-model calculations of the meson properties. However, the confirmation of their presence in the eta mesons could have far-reaching implications on the physics of etas.

REFERENCES

1. R. Koniuk and N. Isgur, Phys. Rev. D 21 (1980) 1868.
2. R.S. Bhalerao and L.C. Liu, Phys. Rev. Lett. 54 (1985) 865.
3. V. Flaminio et al., "Compilation of cross sections I: π^+ and π^- induced reactions", CERN-HERA 83-01.
4. R.M. Brown et al., Nucl. Phys. B 153 (1979) 89.
5. R.A. Arndt, phase-shift solution FP84, private communication.
6. D.J. Herndon et al., LBL report No. UCRL-20030 πN.
7. R.S. Bhalerao, Phys. Rev. C 35 (1987) 1592.
8. Pickup et al., Phys. Rev. Lett. 8 (1962) 329; Collera et al., Phys. Rev. 161, (1967) 1387.
9. F. Wellers and L.C. Liu, unpublished.
10. Q. Haider and L.C. Liu, Phys. Lett. B172 (1986) 257.
11. Q. Haider and L.C. Liu, Phys. Rev. C 34 (1986) 1845.
12. R. Chrien et al., Phys. Rev. Lett. 60 (1988) 2595.
13. B.J. Lieb et al., LAMPF Experiment 1022, to appear in "Progress at LAMPF 1988", Los Alamos National Laboratory Report, LA 11339-PR.
14. G. t'Hooft, Phys. Rev. Lett. 37 (1976) 8.
15. R. Friedberg and T.D. Lee, Phys. Rev. D 18 (1978) 2623.
16. G. Karl, Nuovo Cim. 38A (1977) 315.
17. M. Frank and P.J. O'Donnell, Phys. Rev. D 32 (1985) 1739.
18. R.D. Field and R.P. Feynman, Phys. Rev. D 15 (1977) 2590.
19. G. Wormser et al., Phys. Rev. Lett. 61 (1988) 1057; W. Hofmann, Ann. Rev. Nucl. Part. Sci. 38 (1988) 279.

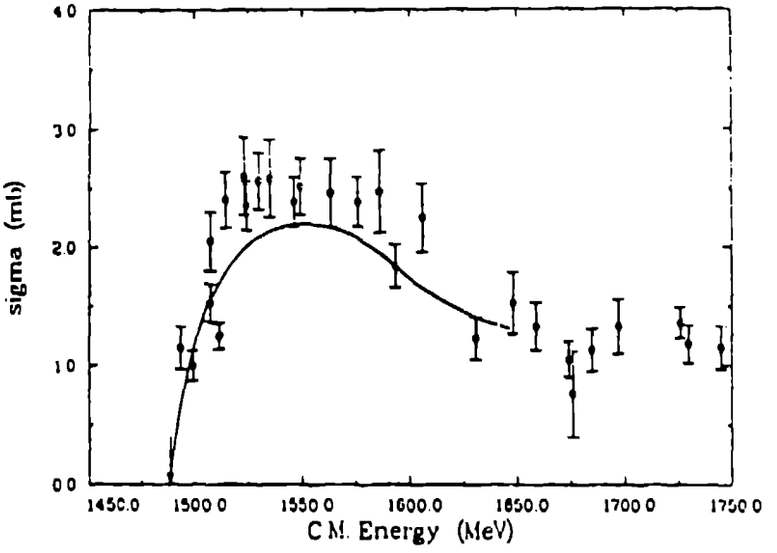

Fig.1 Total cross sections for the $\pi^- p \to \eta n$ reaction. Data are from Ref.3. Curve is the prediction based on the πN phase shifts of Ref.5.

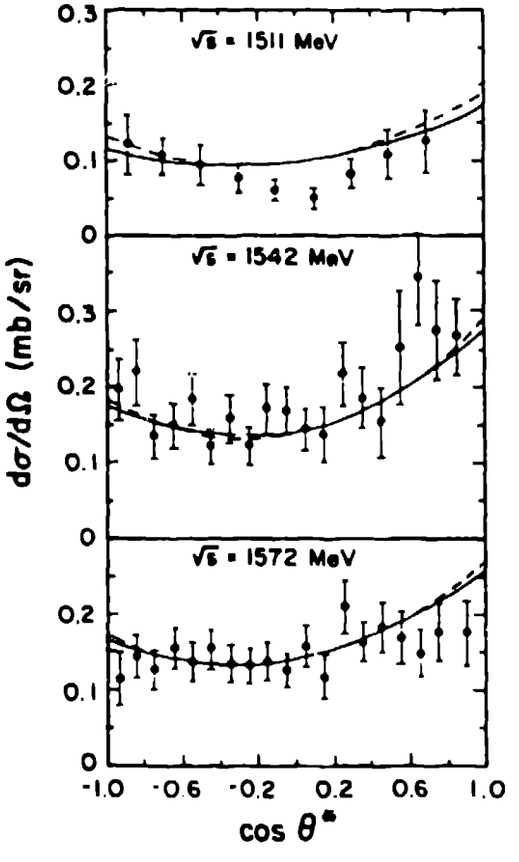

Fig.2 Differential cross sections for the $\pi^- p \to \eta n$ reaction. Data are from Ref.4. Solid (dashed) curves are obtained with the parameters determined from the πN phase shifts of Ref.5 (Ref.6).

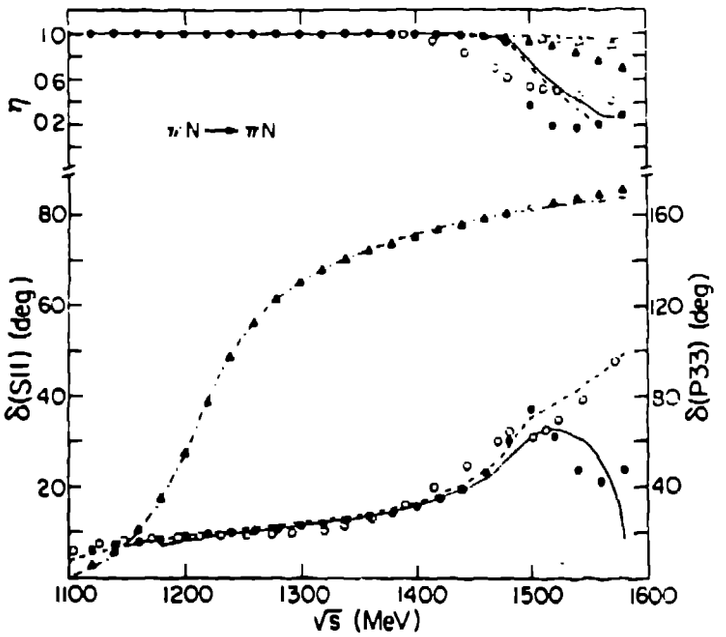

Fig.3 πN phase shifts δ and elasticities η versus c.m. energies. The S11 data of Ref.5 (Filled circles), the S11 data of Ref.6 (open circles), and the P33 data of Ref.5 (filled triangles) and of Ref.6 (open triangles) are compared with the calculations.

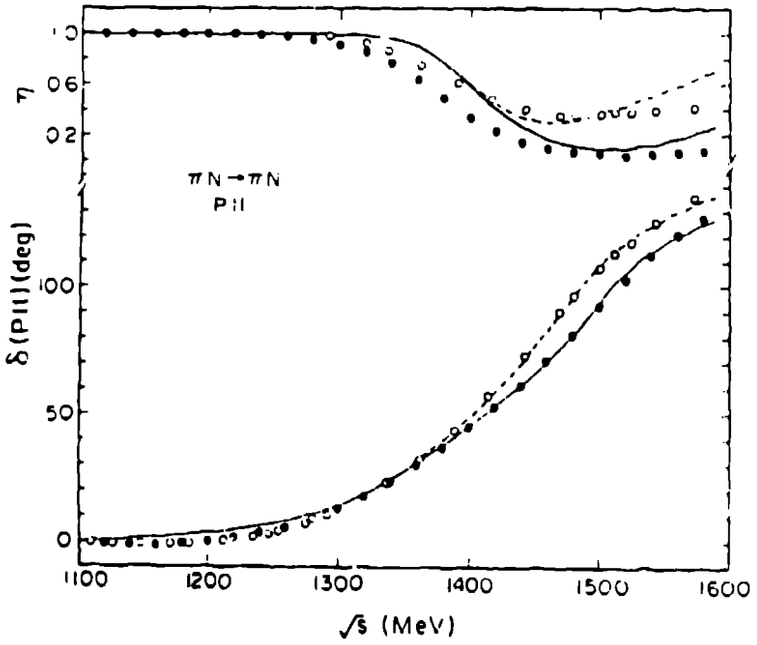

Fig.4 Data and calculations for P11 πN phase shifts and elasticities. Same captions as for Fig.3.

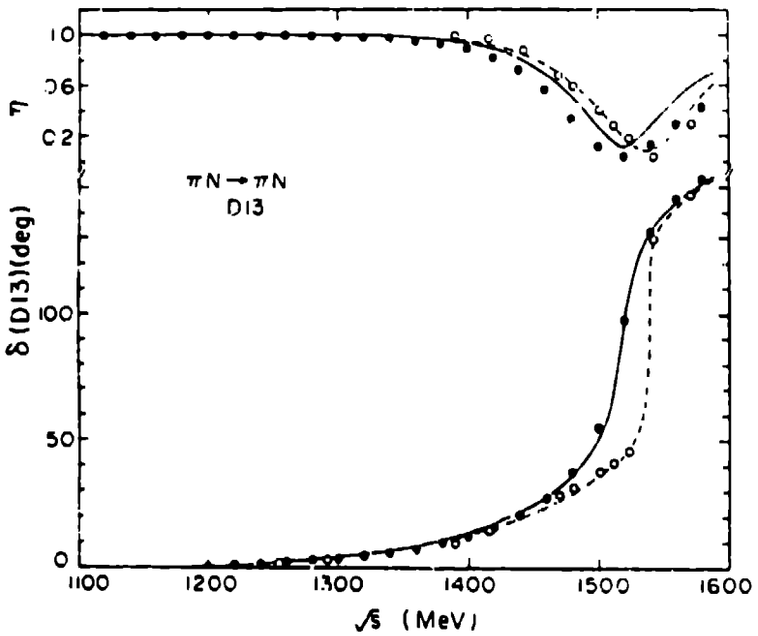

Fig.5 Data and calculations for D13 πN phase shifts and elasticities. Same captions as for Fig.3.

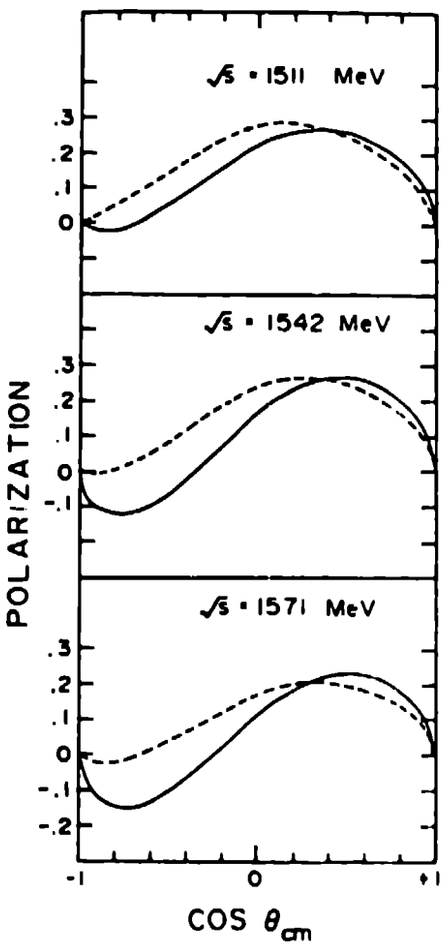

Fig.6 Calculated polarizations Solid (dashed) curves are obtained with the parameters determined from the πN phase shifts of Ref.5 (Ref.6).

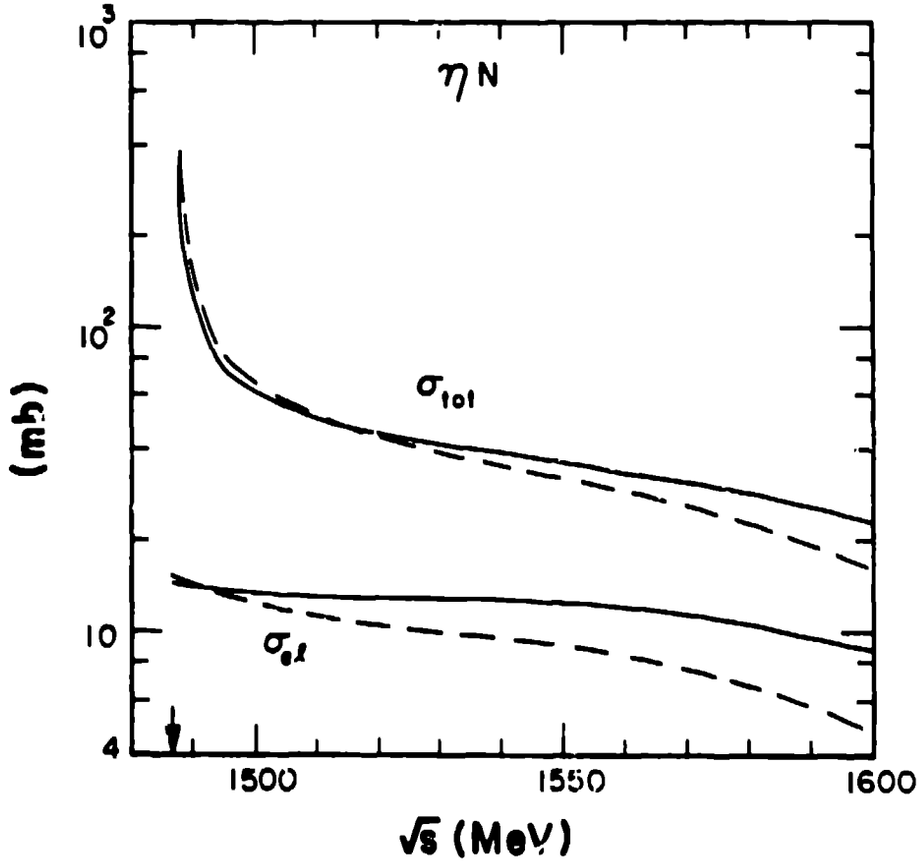

Fig. 7 Calculated eta-nucleon total and elastic cross sections. Same captions as for Fig.6.

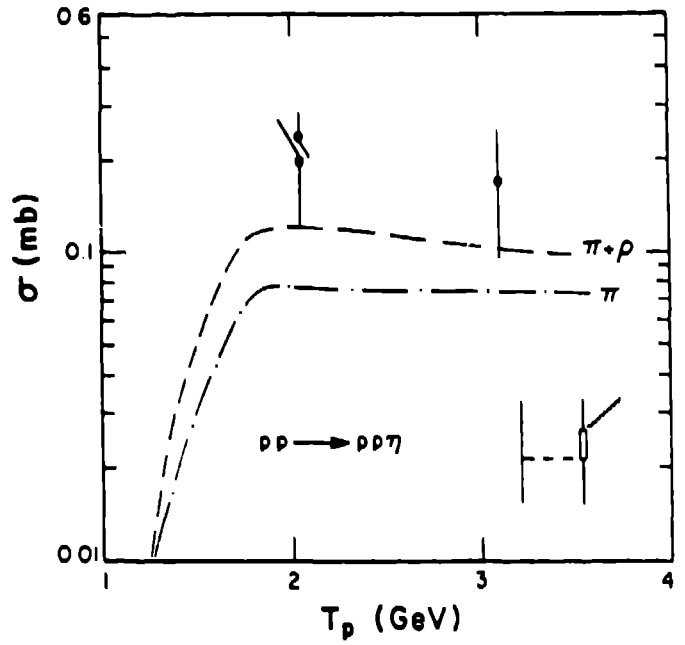

Fig.8 Total cross sections for the pp → ppη reaction.

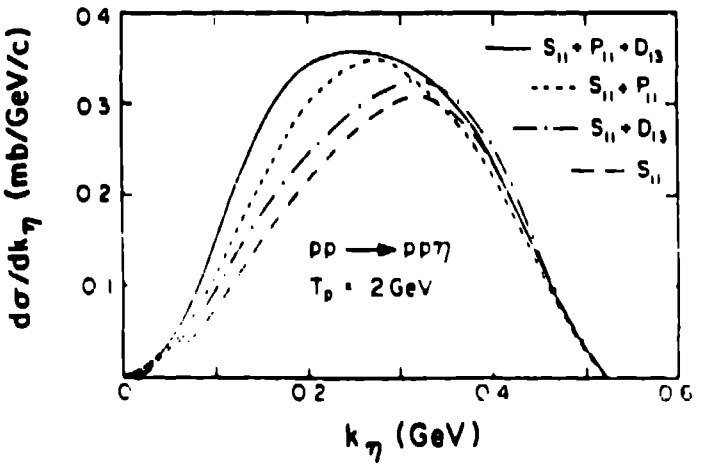

Fig.9 Calculated differential cross sections for the pp → ppη reaction.

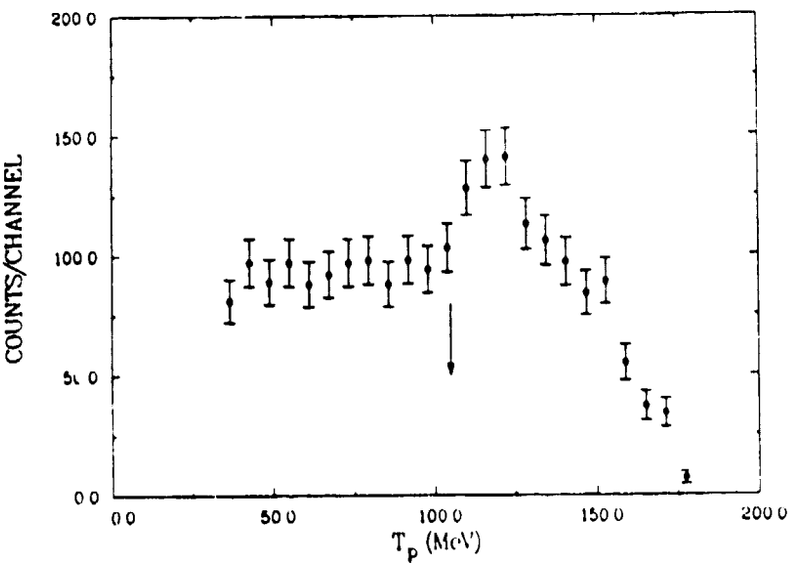

Fig.10 Proton spectrum obtained with triple coincidence measurements of the $^{16}O(\pi^+,pp\pi)$ reaction at $p_{\pi,lab}$ = 657 MeV/c.

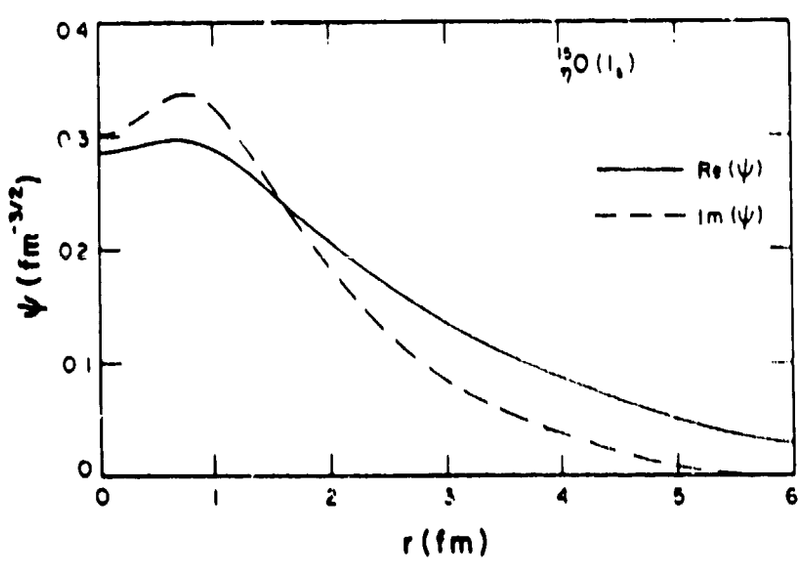

Fig.11 Bound-state wave function of eta in the orbital 1s in ^{15}O.

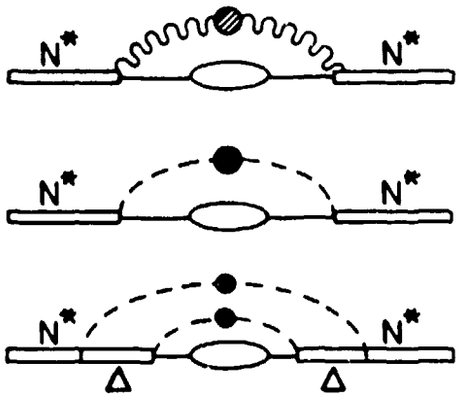

Fig.12 Nuclear medium modifications of the self-energies of an N*.

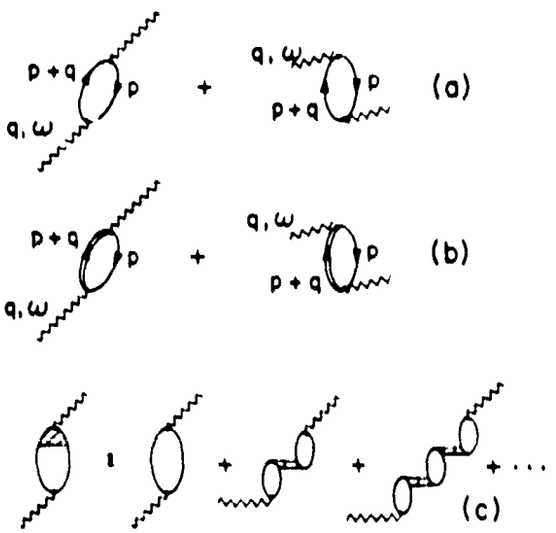

Fig.13 Self-energy insertions to the mesons: (a) Direct and exchange particle-hole contributions; (b) Δ (or N*)-hole contributions; and (c) Renormali- (c) Renormalization of direct particle-hole self-energy by including short-ranged repulsion summed to all orders in the "ring approximation".